Self-Folding Printable Elastic Electric Devices: Resistor, Capacitor, and Inductor

Shuhei Miyashita[1], Laura Meeker[2], Maurice Göldi[3], Yoshihiro Kawahara[4], and Daniela Rus[1]

***Abstract*— This paper presents a methodology and validation of print-and-self-fold electric devices. For printing functional structures for robotic use, we realize electric circuitry based on metallic polyester film (MPF). By exploiting the unique material properties of MPF, we developed fundamental electric devices, namely a resistor, capacitor, and inductor. The developed polyvinyl chloride laminated MPF sheet shows reliable self-folding processes under a heat application, and it configures 3D electric devices. Due to the pre-resolved kinematic design, these devices feature elasticity, making them suitable as sensors and actuators in soft circuits. Here we testify to a self-assembled variable resistor and capacitive strain sensor. An actuation mechanism consisting of a folded contractible coil is also considered and shown. Finally, an RLC circuit obtained from the integration of all the developed devices is demonstrated, in which the coil based actuator is controlled by reading a variable capacitive strain sensor.**

I. Introduction

A technique for "printing" a functional robot is a futuristic dream of many engineers, and success promises to entirely change the method of robot fabrication. Recent progress in the printability of 3D structures has provided engineers with fast and easy access to rapid prototyping techniques, enhancing the speed of development. The challenge now shifts to the printability of the "brain part", namely the electronics and the controlling methods. Toward this end, we develop a method and technique for self-assembling conductive materials to desired functional formations.

Recently, various types of robots have been fabricated through folding processes, inspired by folding-based assembly techniques, such as Origami art work. Roach is a 2.4 g autonomous hexapod robot with a body shape made through folding and assembling processes [1]. Onal et al. developed inchworm robots by patterning a single Polyester sheet and manually folding. [2]. Hawkes et al. achieved the self-folding of an origami structure using a shape memory alloy to provide actuation. [3]. Yasu and Inami demonstrated the self-folding of a robot-like structure in a microwave oven, using a heat-sensitive sheet coupled with a microwave-sensitive aluminum sheet. [4]. Felton et al. achieved the self-folding of an inchworm robot using Shape memory polymer powered by Joule heating [5]. Tolley et al. investigated various types of self-folding methods for robotic applications [6], and Miyashita et al. achieved self-pop-up of a cylindrical structure using global heating [7].

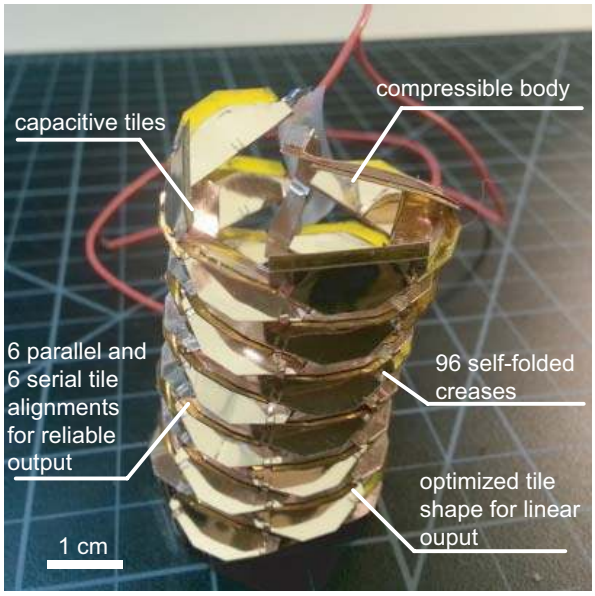

Fig. 1: Self-folded capacitive strain sensor as a variation of the model shown in Section V-C.

A technique for making mm-scale robots using the pop-up method was developed by [8]. A theoretical framework for designing pop-up parallel folds was presented in [9]. A recent series of achievements in folding at MEMS scale was shown in [10]. One-dimensional structure folding using DNA origami was realized in [11], and it was inspired by protein foldings in [12]–[14]. Elastomer-based folding techniques are presented in [15].

Recent advances in realizing soft electronics provide versatility in stretchability, compressibility, twistability, bendability, and deformability for arbitrary shapes of electronics [16]–[20].

Toward the realization of "printing" electronics for robots, this paper investigates a method of print-and-fold for basic electric components with built-in components. The contributions of this paper are:

1) We developed a method of realizing resistance, capacitance, and inductance through the use of a metalized polyester sheet.
2) We advanced a technique of sheet self-folding and achieved self-assembly of conductive material.
3) We designed a variable resistor and capacitive strain

[1]Computer Science and Artificial Intelligence Laboratory, MIT. 32 Vassar street, Cambridge, MA, 02139, USA. [2]Department of Mechanical Engineering, MIT. [3]Department of Biopsychology, University of Zürich, Switzerland. [4]Department of Information and Communication Engineering, The University of Tokyo, Japan. {shuheim}@csail.mit.edu

This research was conducted in the Distributed Robotics Laboratory at CSAIL, MIT. Support for this work has been provided partially by NSF grants 1240383 and 1138967, and the Swiss National Science Foundation Fellowship Grant PBZHP2-133472.

sensor as examples of self-assembled functional electric devices and attained an origami coil actuation mechanism.

4) We combined the sensor and actuator to show that the new devices can be composed.

II. General Principles & Methods

Our technical approach for realizing resistors, capacitors, and inductors exploits the conductivity and resistivity using the structure or geometry of material sheets. In particular, we use $50.1\,\mu$m thick isotropic aluminum coating (one side) polyester film (MPF, Mylar).

A specific resistance can be attained by varying the material's geometry. Thus, a 3×3 cm square cut of MPF has about $\approx 4.4\,\Omega$. The resistance can be linearly increased by lengthening the MPF, and inversely, can be decreased by narrowing the width of the sheet. By translating this cutting-and-regulating approach to folding methods, we can realize elastic resistors of various resistances (the limit is given by the geometry).

Since the resistance of the MPF is relatively low as the sheet resistance $\approx 1\,\Omega$, it can be used as a conductive cable in short-length circuitry. Because the resistivity is not as negligible as that of copper, such a conductive cable is more suitable for digital circuits.

Capacitors can be obtained using two electrically isolated MPF. Capacitance of two parallel MPF is proportional to the surface area and inverse proportional to the distance between the plates. Thus, the capacitance magnitude can be regulated by the arrangement and the geometry of the paired surfaces. In a folding fashion, we realized a capacitor by pairing angled MPF surfaces, where a shared edge forms the hinge between the tiles. This way, for example, two square MPF of $2\times2\,\text{cm}^2$ spanning an angle of $45\,^\circ$ with a 2 mm gap from the shared edge exhibits a capacitance of ≈ 0.4 pF. Due to the fact that the capacitance increases roughly proportional to the surface area, the size of the device influences the capacitance magnitude.

The inductor is the resistivity of a structure against the current change, and the typical type is also known as a coil. To show the capability of self-assembly in realizing folded 3D structures that satisfy the topology of an inductor, we designed a self-assembled solenoid coil. The coil can create a magnetic field within a certain volume, which can subsequently be used for actuation mechanisms, as introduced in Section VI-C. The inductance is determined by the number of turns as well as the geometry (size). For instance, an MPF solenoid coil with radius 16 mm, height 6 mm, and 5 turns theoretically shows $2.10\,\mu$H.

Tests with an MPF-based inductor showed that it can sustain up to an $\approx$ 300 mA current before an instant loss of conductivity occurs due to changes in the characteristic of the polyester layer produced by heat. MPF maintains conductivity as well as resistivity given the non-harsh iterative foldings. The sheet can withstand a temperature range of -45°C to 148°C, making the material a poor candidate for soldered connections. Therefore, conductive connections in the circuit were made using conductive tape, conductive epoxy glue, and mechanical clippings.

III. Self-folding MPF by Global Heat

Among the various types of existing self-folding techniques, we have developed a simultaneous multi-crease self-folding technique based on global heating with a heat sensitive sheet (Poly-Vinyl Chloride; PVC, Shrink Bag, shrinking temperature: $65\,\text{C}^\circ \sim 75\,\text{C}^\circ$) [7]. Fig. 2 shows the design and fabrication processes. After determining the desired variable

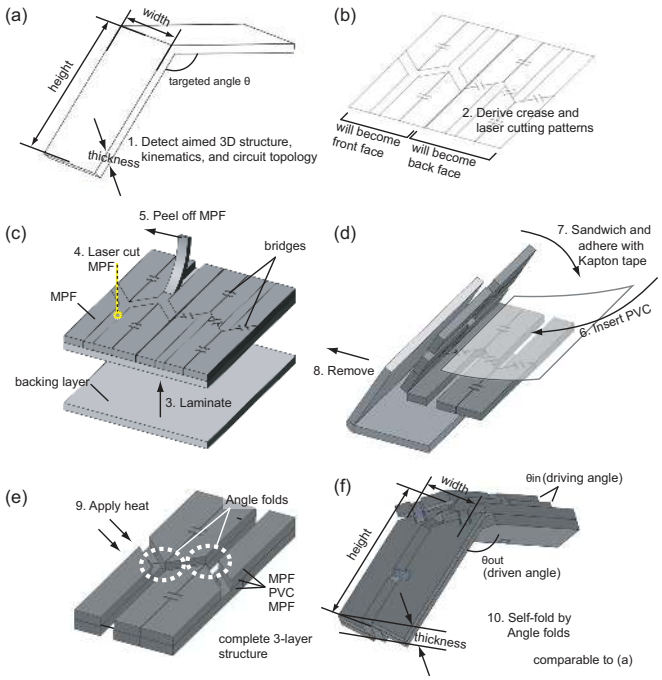

Fig. 2: Design, fabrication, and self-folding processes.

properties, such as the folded sheet structure, kinematics, and circuit topology, we derived the crease pattern for self-folding considering all conditions (Fig. 2 (a)→(b)). The unique characteristics of this approach are: (1) it has a three-layer structure in which creases bend to the wider opening sides of gaps (Fig. 2 (d)(e)), (2) the geometry of the surface, height, width, and thickness in Fig. 2 (a) can be encoded in Fig. 2 (b) and reflected in Fig. 2 (f), (3) there are driving (or input) angles and driven (output) angles, and the accurate driven angles are roughly controlled by the driving angles (using pop-up Angle folds) (Fig. 2 (f)), (4) with the exception of the laser cutting step, the entire process is completed without the assistance of equipment, (5) the conductive surface in the self-folded 3D structure can be exposed or hidden depending on which side of the MPF faces up in the lamination phase in Fig. 2 (c), and (6) further lamination of the layers is possible to provide additional functionalities. Conductivity is maintained via "bridges" that link the conductive tiles (Fig. 2 (c)), which also keeps the tiles from coming closer and bending in the wrong direction when heated. Note that due to the torque required, bridges can only be placed over mountain folds. The total thickness

of the self-folding sheet is 0.3 mm. See [7] for more details about fabrication.

IV. Resistance

A. Device

Fig. 3 shows one of the images of resistor (MPF resistor). In order for the resistor to attain physical compressibility and

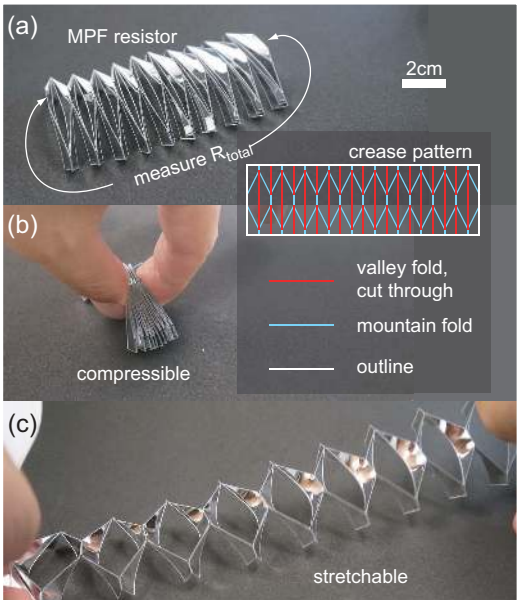

Fig. 3: Designed MPF resistor at normal length (a), compressed (b), and stretched (c).

stretchability in one direction, we combined slit traces [21] and Angle folds, and we manually folded as described in the crease pattern. This way, the structure features an excellent extension rate of over 100 times ($\approx$ 118 times) and shows good tensile strength.

B. Model

This section models the MPF resistor. For 3D resistance, $R = \frac{\rho}{l_t}\frac{l_h}{l_w} := R_s\frac{l_h}{l_w}$, where ρ is the resistivity intrinsic to the material, l_t is the unknown thickness, l_h is the height, l_w is the width of the material, and R_s is the sheet resistance. We measured the resistivity of the material using the Van der Pauw method (the sample thickness is much less than the width and length of the sample [22]). The Van der Pauw method can be utilized by applying a current between two adjacent corners of a rectangular sheet and measuring the voltage across the opposite corners to obtain a particular resistance value. $R_v = 0.208$ is the resistance measurement when vertically applying the current between the two corners on either the left or the right edge and measuring the voltage across the opposite edge. $R_h = 0.204$ is the resistance measurement when horizontally applying the current between the two corners of either the top or the bottom edge of a rectangular sheet and measuring the voltage across the opposite edge. We obtained the sheet resistance $R_s = 0.933\,\Omega$ by iteratively solving the Van der Pauw formula $e^{-\pi\frac{R_v}{R_s}} + e^{-\pi\frac{R_h}{R_s}} = 1$ for R_s.

Fig. 4 shows the plot of experimentally measured resistances depending on the different width (l_w) to height (l_h) ratios of the rectangular MPF. By fitting the curve, we obtain

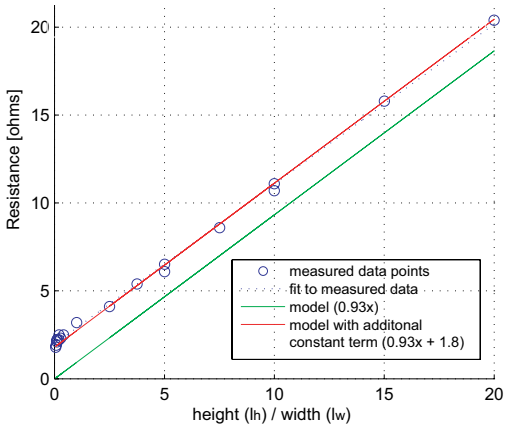

Fig. 4: Resistance of MPF with different geometries.

$R = 0.93\frac{l_h}{l_w} + 1.8$, which shows a similar value to what we obtained from the Van der Pauw method, and we will use this model for rectangular resistors.

As our idea is to embed resistance within a (self-)folded structure, we wish to estimate the resistance when bridges are included in a pattern (ref. Fig. 2). Fig. 5 illustrates various resistances made by cutting $3 \times 3\,\text{cm}^2$ MPF and varying the width (l_w) and height (l_h) of the bridges. By

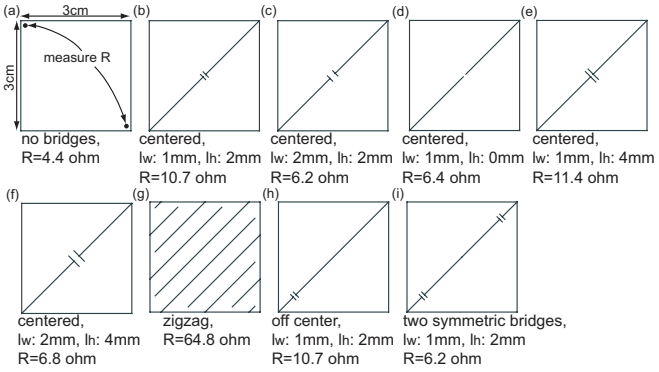

Fig. 5: Various resistances realized by cutting $3 \times 3\,\text{cm}^2$ MPF.

comparing (b) and (h), it can be derived that the position of a bridge does not affect the resistance. We hypothesize that the resistance of a sheet, R_{total} can be modeled as connections of the i-th ($i \in \mathbb{N}$) surfacial geometric portion that attributes the resistance R_i connected in parallel and in series. For example, the resistance i serial resistances, each composed of one surfacial portion, can be calculated as $R_{total} = \sum_i R_i$ where R_i is the resistance of the i-th surface. For example, the total resistance of the structure in Fig. 5 (b) can be approximately calculated as the sum of the resistance of Fig. 5 (d) and the $1 \times 2\,\text{mm}^2$ bridge portion. With this model, our calculation estimates that the R_{total} of Fig. 5 (b) is $10.18\,\Omega$, while the measured value was $10.7\,\Omega$ ($\approx$ 5.1% error). In the same way, the model

estimates the R_{total} of Fig. 5 (e) as $12.0\,\Omega$, where the measured value was $11.4\,\Omega$ ($\approx 5.0\%$ error). Considering that the measured resistances are relatively small and are not stable when measured with a multimeter, the derived model can be considered to reasonably estimate the resistance value. In practice, with a surface area $3 \times 3\,\text{cm}^2$, our estimation of the achievable resistance range is $\approx 4\,\Omega - 3.2\,\text{k}\Omega$, with the assumption that the thinnest width obtainable with our laser cutter is $l_w = 0.5\,\text{mm}$.

C. Experiment

This section demonstrates self-folding of a variable resistor as an example to show the capability of our system. The idea was to circulate electrically connected tiles around the structure and to manually short the circuit, thereby changing (reducing) the resistance in steps (four steps in this case). The tiling pattern and the path of electrical conductivity (depicted with blue lines) are shown in Fig. 6 (a). We show tiles from the front surface in red and from the back surface in blue. This circuit topology allows for coupled faces to be electrically connected in series, and the self-folded 3D geometry forms a scaling zigzag pattern for easy pinching. Fig. 6 (b) shows snapshots of the conducted self-folding

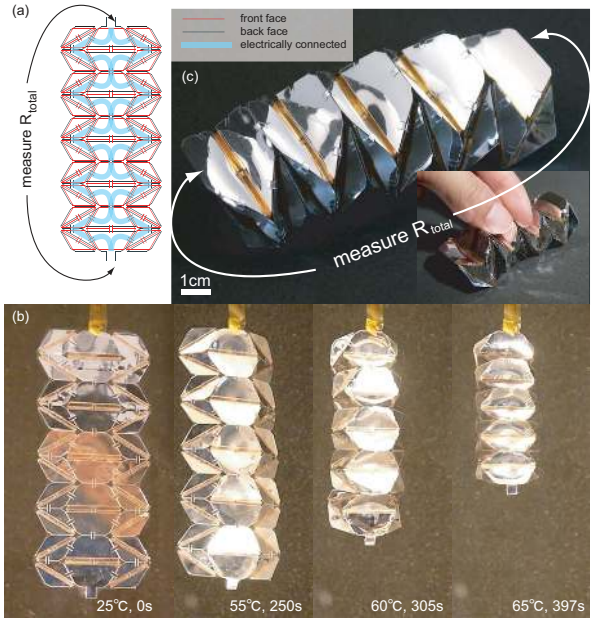

Fig. 6: Self-folded MPF variable resistor. (a) Designed crease pattern with front and back sides overlaid. (b) Self-folding process in an oven. (c) The outlook of the self-folded variable resistor and an example of usage in the small window.

process. The reliable self-folding process, which took about five and a half minutes, is shown. Fig. 6 (c) shows the self-assembled MPF variable resistor. Due to the kinematics of the structure, linearly aligned tiles on the top surface can be shorted by hand, as shown in the small window in 6 (c). The structure possesses elasticity, and it recovers its original posture when the external force is removed. The measured resistances are $83.56 \pm 1.44\,\Omega$ (with no pinches), $74.48 \pm 2.20\,\Omega$ (with 1 of 4 scales pinched), $62.49 \pm 1.86\,\Omega$ (2 pinches), and $49.94 \pm 0.94\,\Omega$ (3 pinches) (sample number = 8). By approximating trapezoid shapes to the similar ratios' rectangles, our model roughly estimates the resistance with no pinches as $\approx 90.4\,\Omega$.

V. Capacitance

A. Model

Fig. 7 (a) and 7 (b) show a schematic representation of a capacitor, which is composed of identically shaped paired angled MPF tiles, in a side view in (a) and an angled view in (b). Each tile is made up of two isosceles triangular surfaces, while the conductive surfaces, which are colored in red, can have a trapezoid shape. Here, r_1 and r_2 are the length of the non-conducting parts of the upper and lower tiles measured from their common hinge, respectively, and l_1 and l_2 are the height of the aluminum coated conductive part of respective conductive surfaces ($\because r_n + l_n \leq$ height of tile; $n \in [1, 2]$).

The thickness of the tiles, $0.05\,\text{mm}$, is denoted as $\frac{T}{2}$, and the angle of the outward facing tip of each tile is given by ϕ. The capacitance of the tiles varies in accordance with the relative angle between them, which is given by θ. The metallic faces are only connected through the scaffolding and remain electrically isolated. When the shapes of the upper

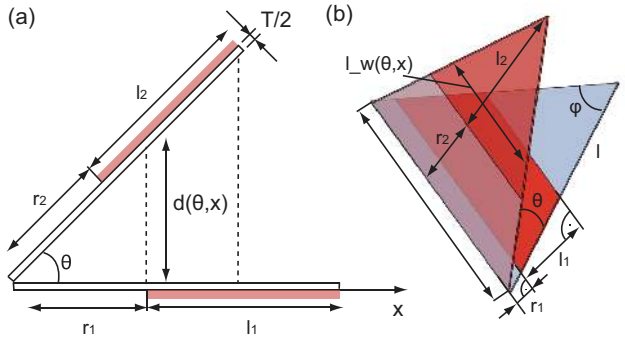

Fig. 7: Capacitor for a folding structure. Schematics in a side view (a) and in an angled view (b). Conductive portions are shown in red and non-conductive portions in blue.

and lower tiles are identical, namely $r_1 = r_2 = r$ and $l_1 = l_2 = l$, the capacitance C at an angle θ by taking the x-axis along the bottom tile is:

$$\begin{aligned} C(\theta) &= \varepsilon_0 \varepsilon_r \int_r^{(r+l)} \frac{l_w(\theta, x)}{d(\theta, x)} dx \\ &= \frac{\varepsilon_0 \varepsilon_r \tan\frac{\phi}{2}}{\tan\theta} \cdot \\ &\quad \left((r+l)\ln\left(\frac{(r+l)\cos\theta}{r} - (r+l) + \frac{r}{\cos\theta}\right)\right), \end{aligned} \tag{1}$$

where $\varepsilon_0 = 8.85 \times 10^{-12}\ \text{Fm}^{-1}$ and $\varepsilon_r = 1.00059$ are the absolute permittivity and relative permittivity of air, respectively, $l_w(\theta, x)$ is the width of the conductive plate, and $d(\theta, x)$ is the distance between the two plates at position x.

B. Shape Optimization for Linear Output

In this work, we plan to use the capacitance change as a sensor. In this respect, the high degree of nonlinearity across the range of $\sin\theta$ becomes an issue. We have therefore attempted to optimize the shape of the tiles, in order for the capacitance to exhibit linear behavior with the change of $\sin\theta$. To this end, we modeled the capacitance with the additional geometric variables of r_1 and l_1 for the top tile, and r_2 and l_2 for the bottom tile, as:

$$
\begin{aligned}
C \;=\; & \epsilon_0\epsilon_r \tan\frac{\phi}{2}\Bigg[(r_2+l_2)\cot\theta\cdot \\
& \ln(\min(r_1+l_1,(r_2+l_2)\cos\theta)\sin\theta+T\cos\theta) \\
& +T\frac{\cot\theta}{\sin\theta}\ln(\min(r_1+l_1,(r_2+l_2)\cos\theta)\cdot \\
& \sin\theta+T\cos\theta))-\frac{\min(r_1+l_1,(r_2+l_2)\cos\theta)}{\sin\theta} \\
& -(r_2+l_2)\cot\theta\cdot\ln(\max(r_1,r_2\cos\theta)\cdot \\
& \sin\theta+T\cos\theta)-T\frac{\cot\theta}{\sin\theta}\cdot \\
& \ln(\max(r_1,r_2\cos\theta)\sin\theta+T\cos\theta)) \\
& +\frac{\max(r_1,r_2\cos\theta)}{\sin\theta}\Bigg]. \qquad (2)
\end{aligned}
$$

We optimized the capacitor to exhibit linear behavior in a range of $30^\circ \le \theta \le 60^\circ$. ϕ was set to 120°, drawn from our previous model in [7]. T was set to 0.05 mm and was determined by the material used. While r_1 remained fixed at 3 mm, our tuning variables l_1 and r_2 varied from 1 mm to 26 mm and from 3 mm to 29 mm, respectively. We correlated the change of capacitance across $\sin\theta$ (Pearson's correlation) with a linear change in capacitance of the same magnitude. To this end, we optimized l_1 and r_2 to find the highest linear correlation to the change of $\sin\theta$.

Fig. 8 (a) and Fig. 8(b) show a 3D plot of the capacitances for varying l_1 and r_2. We indicate the most linear solution with red lines. From this model, we obtained the values $l_1 = 17.6$ mm and $r_2 = 14.7$ mm as the optimized geometry.

We validated the results by experimentally measuring the capacitance value with the same arrangement. Here, we tested two configurations: (1) both tiles with fully overlapping triangles, namely $r = 3$ mm, and (2) with the obtained optimal geometry regarding linearity, as produced by our model. The comparison between experimental and modeled results are shown in Fig. 9. We plot the data in different scales, as our model does not consider tile thickness and *edge effects* are not modeled, and thus the absolute values of capacitances are different between the model and the real measurement. The full triangle pattern shows a higher capacitance range than the optimal design. As suggested by the model, the optimized design is shown to be linear across the optimized range of $30^\circ \le \theta \le 60^\circ$.

C. Experiment

Following the basic idea for realizing an MPF capacitor, we have produced a self-assembling capacitive strain sensor.

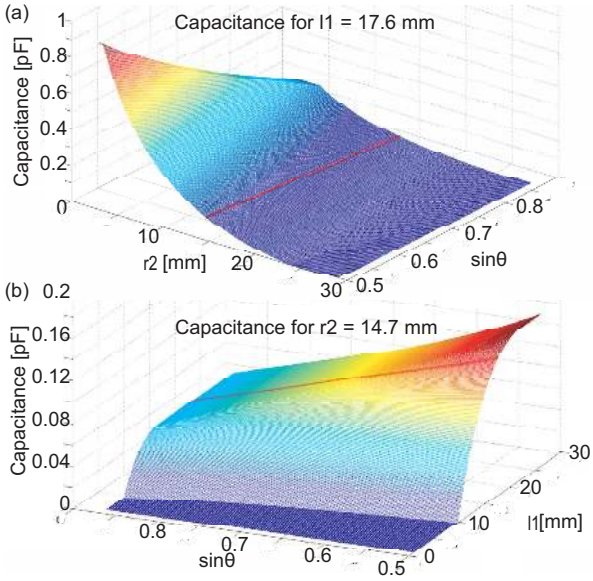

Fig. 8: Capacitances for (a) fixed l_1 and varying r_2 and (b) fixed r_2 and varying l_1. The fixed l_1 and r_2 are fixed to the optimal solution with respect to linearity. The red lines indicate the optimal solution.

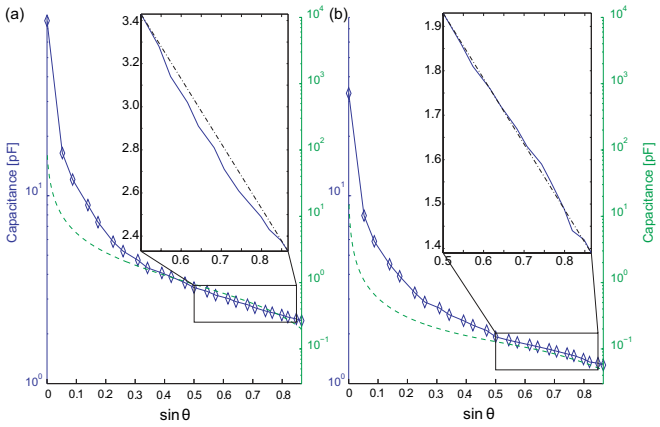

Fig. 9: Experimental (solid lines) and modeled (dashed lines) capacitances of (a) triangular and (b) optimized capacitor plates. An improvement in the output linearity can be recognized (note that the small windows are plot in normal scale, with a support of linear dash-dotted lines for reference).

The designed crease pattern, which is shown in Fig. 10 (a), was developed based on the X-form spans folding pattern. The tiling pattern and the connections between tiles via bridges satisfy a compressible structure when self-assembled, and thus they can be used for strain sensors with reflected capacitance values, as well as being appropriate circuit topology for five parallel capacitors. The self-assembly process is shown in Fig. 10 (b). Through global heating, the sheet reliably folds 100 creases simultaneously and self-assembles into the intended 3D strain sensor. Note that all the necessary circuitry has also been completed, and the structure is ready to use. Due to the kinematics of the structure, it can be compressed to the range shown in the small window in Fig. 10 (c). When the force is released, the structure expands

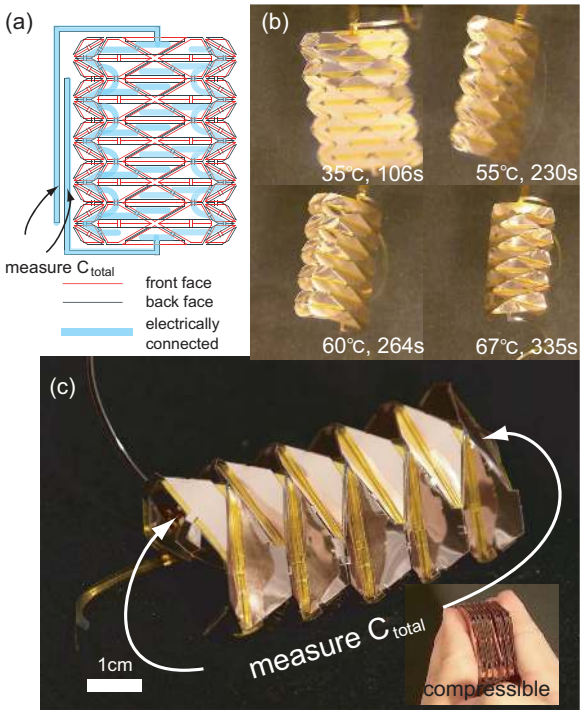

Fig. 10: Self-assembly of a capacitive strain sensor made in an oven. The scale of the individual capacitance elements was reduced to 50% from the single elements described in the previous section.

back to its original length.

We plot the capacitance of the original triangular and optimized tile shapes against the strain of the sensor in Fig. 11. The blue line represents the data for the triangular

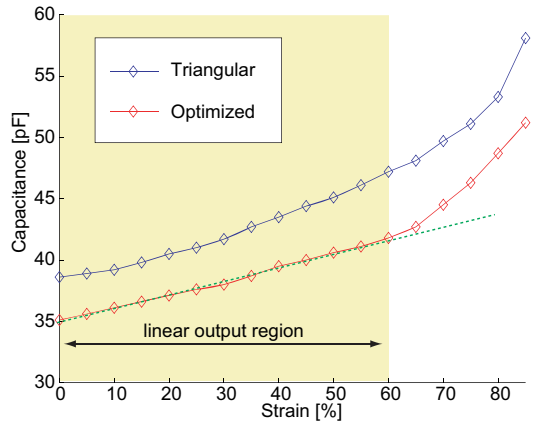

Fig. 11: Capacitance of self-folded strain sensor. Experimental results of triangular (blue) and optimized (red) tiles.

capacitor plates, and the red line represents the data for the optimized capacitor plates. Within the marked region, the sensor shows linear behavior (as can be seen by the green overlay), with the optimized configuration having a slight improvement in linearity over the triangular configuration. It can be seen that 20% of the change in capacitance can be controlled through compression of the structure, making it a functioning strain capacitive sensor.

VI. Inductance

A. Model

We employed Harold Wheeler's formula [23] for calculating the inductance of a single-layer coil (L), due to the reason that this formula smoothly connects the "short coil" and "long coil" approximations, allowing for an accurate model for a spectrum of shapes.

$$L = \mu_0 n^2 l_R \left[\ln\left(1+\frac{\pi l_R}{l_H}\right) + \left(2.3+1.6\left(\frac{l_H}{l_R}\right)+0.44\left(\frac{l_H}{l_R}\right)^2\right)^{-1}\right], \quad (3)$$

where μ_0 is the permeability of free space, n is the number of turns, l_R is the radius of the coil, and l_H is the height of the coil.

First, we determined the crease pattern for self-assembly. Fig. 12 (a) shows the designed crease pattern. The folding pattern was designed such that (1) it will generate a spiral structure of six folds for one turn, (2) the wire part will attribute a certain thickness for stable overlap, and (3) it will electrically connect all the tiles for current flow along the spiral structure. It was designed to configure into a hexagonal coil of 5 turns, 16.0 mm radius, and a height of 6.0 mm. Note

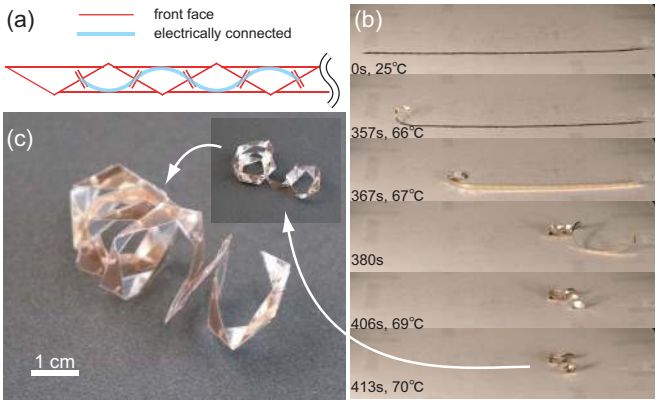

Fig. 12: Self-folding MPF coil: (a) crease pattern, (b) self-assembly process, and (c) MPF solenoid coil (we further manually added pressure to the creases).

that the density of turns can be changed by regulating the gap widths of the valley folds, which results in variation of the final height. As the folding angle approaches 180°, the density reaches its maximum value and the magnetic field increases for a given current.

B. Experiment

Fig. 12 (b) shows the self-assembly process of the MPF solenoid coil. Due to the torque requirement for lifting the lengthy structure, we placed the self-folding sheet onto a plate in an oven. At around 65°C, the formation of a spiral shape was observed. The self-assembly process ended when the temperature reached 70°C. The folding, from beginning to end, only took about a minute and a half. We manually wimpled some of the creases and obtained the final structure,

as shown in Fig. 12 (c). Note that due to the kinematics, the coil can be compressed. Wheeler's formula predicted $L = 0.52\,\mu$H, though the value was too small to measure with an LCR meter.

C. Application to Actuation Mechanism

In order to demonstrate the effect of the magnetic field generated by a folded solenoid coil, we further investigated the possibility of realizing an actuation mechanism. The basic idea was derived from the concepts behind a voice coil, in which an electrical coil generates a force that acts on a permanent magnet, generating sound. Our approach was to have a compressible origami coil with two ferrous cylindrical cores suspended inside both ends. When the current was run through the coil, the ferrous cores within become magnetized in the same direction and attracted each other (Fig. 13 (a)). The coil contracted due to the attractive force between the ferrous cores. Part of this idea can be found in microrobotics [24], where a microrobot equipped with two soft magnets changed the magnets' distance using an externally applied resonant magnetic field, thereby attaining locomotion.

In practice, MPF was unable to run sufficient current for actuation at this scale. We therefore utilized a manually folded 24-winding copper-based origami coil with the same folding geometry pattern as Fig. 12, insulating the conductivity between layers using Kapton tape. For the cores,

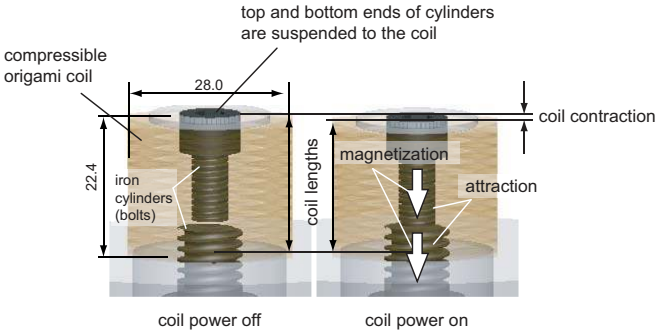

Fig. 13: Concept and schematics of origami-coil actuation mechanism. Units are in mm.

we used a 6.3 mm diameter ferrous cylinder (bolt) for the upper end and an 11.1 mm diameter ferrous cylinder for the lower end. While measurements with the LCR meter showed $L = 4.6\mu$H, Wheeler's formula predicted $L = 5.0\mu$H.

Fig. 14 shows the magnetic flux density generated by the origami coil. A linear increase in the strength can be seen in proportion to the current increase.

Fig. 15 shows the compression of the origami coil. Upon applying current to the origami coil, the structure compressed due to the attraction between the cores, and millimeter-level actuation was achieved. At 5 A of current, a $\approx$ 0.8 mm contraction ($\approx$ 3.57% compression) was observed in the structure. We are supposing that the contraction level can be improved using a thinner insulation layer, a larger number of coil windings, and a higher current application. The nonlinearity against an increase in current comes from the effect of the distance between the two cores, whose magnitude of

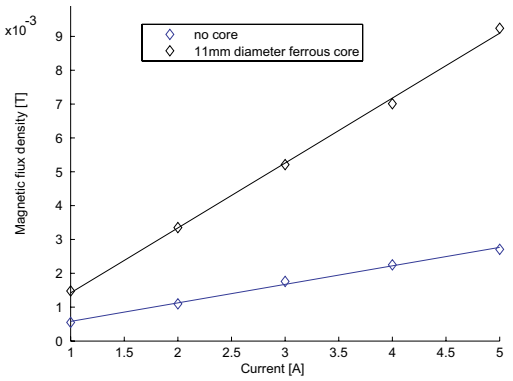

Fig. 14: Magnetic field density generated by manually folded copper origami coil.

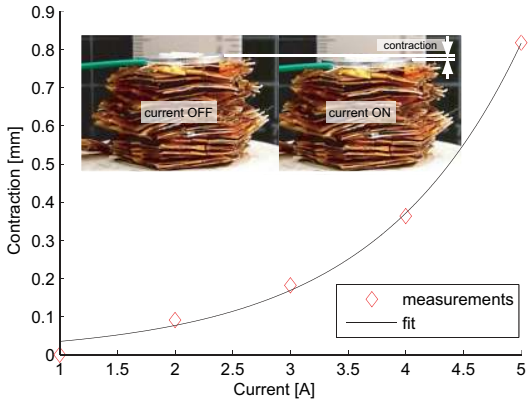

Fig. 15: Contraction measured with different current amounts.

force is inversely proportional to the relative distance to the power of four. However, while predicting the compression rate to obtain a precise model of the spring constant of our origami coil is required, this is out of the scope of this paper.

VII. Integration of Devices

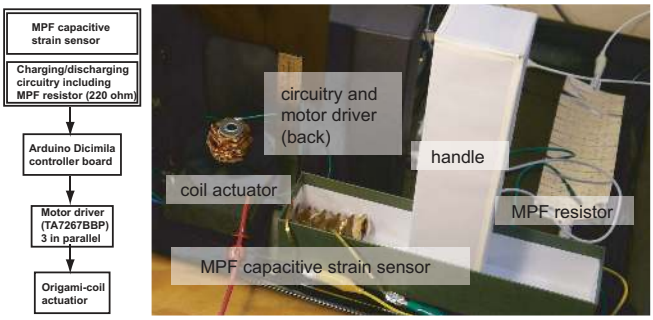

Fig. 16: Experimental setup and control diagram. The demonstration is shown in the supplemental video.

We read the MPF capacitive strain sensor data with an Arduino contoller board with a support of two resistors (10 MΩ and 220 Ω), and we controlled the magnetic field strength generated by the origami-coil actuator as the linear output of the strain value of the MPF capacitive strain sensor. We incorporated the MPF resistor into the circuit as the 220 Ω

resistor. A range of 30 to 60 pF of optimized capacitance, regulated manually through compression, is linearly mapped to a 0 to 5 A current range in order to power the origami-coil actuator. Fig. 16 shows the experimental setup and the control diagram. With the compression of the capacitive strain sensor, we observed the compression of the origami-coil actuator together with the generation of a magnetic field from the origami-coil. The demonstration, which are shown in the supplemental video, proves the combinatorial usage of developed devices.

VIII. Discussion & Conclusion

In this paper, we presented the method, development, and usage of self-folding electric devices. We combined MPF and a heat-sensitive shrinking film to self-fold structures by applying global heat. Thus, the folded structure is characterized by both conductivity and elasticity, making it appropriate for elastic electric devices, such as a variable resistor, a strain sensor, and a voice-coil based actuator. We optimized the tile shape of the capacitive sensor and improved its output linearity with respect to the deformation level of the structure. The result indicates that the compulsory circuit topology can co-exist with the capability of self-assembly while satisfying the required kinematics. We further integrated these devices and demonstrated a basic sensor-motor control by reading the strain of the capacitive sensor and regulating the folded coil-based actuator.

The novel electric devices have unique properties due to the underlying material and the fabrication process. The developed MPF resistors have limitations in terms of the resistance output compared to normal resistors, which attain a few mega ohm keeping their size. Nonetheless, the structure features elasticity and tangibility in fabrication. The maximum value of the MPF capacitor is in the pF range. This implies that an appropriate use for these capacitors is as sensors, as they showed reliable and repeatable outputs. The limited current capacity that the MPF coil currently supports is not a negligible issue, but it will be addressed further in order to create actuation mechanisms of significant output.

In summary, the methodology showed the potential of using a conductive polyester sheet for electric devices by means of a simple and cheap printing-based fabrication and a reliable self-folding process. In addition to pursuing the creation of a wide functional platform based on the presented methodology, we will continue to improve the entire automation process.

References

[1] A. M. Hoover, E. Steltz, and R. S. Fearing, "RoACH: An autonomous 2.4g crawling hexapod robot," in *IEEE/RSJ International Conference on ntelligent Robots and Systems (IROS)*, 2008, pp. 26–33.

[2] C. D. Onal, R. J. Wood, and D. Rus, "Towards printable robotics: Origami-inspired planar fabrication of three-dimensional mechanisms," in *IEEE International Conference on Robotics and Automation (ICRA)*, 2011, pp. 4608–4613.

[3] E. Hawkes, B. An, N. M. Benbernou, H. Tanaka, S. Kim, E. D. Demaine, D. Rus, and R. J. Wood, "Programmable matter by folding," *Proceedings of the National Academy of Sciences*, vol. 107, no. 28, pp. 12 441–12 445, 2010.

[4] K. Yasu and M. Inami, "Popapy: instant paper craft made up in a microwave oven," in *The 9th international conference on Advances in Computer Entertainment*, 2012.

[5] S. M. Felton, M. T. Tolley, C. D. Onal, D. Rus, and R. J. Wood, "Robot self-assembly by folding: A printed inchworm robot," in *IEEE International Conference on Robotics and Automation (ICRA)*, 2013, pp. 277–282.

[6] M. Tolley, S. Felton, S. Miyashita, L. Xu, B. Shin, M. Zhou, D. Rus, and R. Wood, "Self-folding shape memory laminates for automated fabrication," in *IEEE/RSJ International Conference on Intelligent Robots and Systems (IROS),*, 2013.

[7] S. Miyashita, C. D. Onal, and D. Rus, "Self-pop-up cylindrical structure by global heating," in *IEEE/RSJ International Conference on Intelligent Robots and Systems (IROS)*, 2013.

[8] J. Whitney, P. Sreetharan, K. Ma, and R. Wood, "Pop-up book mems," *Journal of Micromechanics and Microengineering*, vol. 21, no. 11, p. 115021, 2011.

[9] Z. Abel, E. D. Demaine, M. L. Demaine, S. Eisenstat, A. Lubiw, A. Schulz, D. L. Souvaine, G. Viglietta, and A. Winslow, "Algorithms for Designing Pop-Up Cards," in *30th International Symposium on Theoretical Aspects of Computer Science (STACS 2013)*, ser. Leibniz International Proceedings in Informatics (LIPIcs), N. Portier and T. Wilke, Eds., vol. 20. Dagstuhl, Germany: Schloss Dagstuhl–Leibniz-Zentrum fuer Informatik, 2013, pp. 269–280. [Online]. Available: http://drops.dagstuhl.de/opus/volltexte/2013/3940

[10] N. Bassik, G. M. Stern, and D. H. Gracias, "Microassembly based on hands free origami with bidirectional curvature," *Applied Physics Letters*, vol. 95, pp. 091 901–1–091 901–3, 2009.

[11] P. W. K. Rothemund, "Folding DNA to create nanoscale shapes and patterns," *Nature*, vol. 440, no. 7082, pp. 297–302, 2006.

[12] T. D. Clark, M. Boncheva, J. M. German, M. Weck, and G. M. Whitesides, "Design of three-dimensional, millimeter-scale models for molecular folding," *Journal of the American Chemical Society*, vol. 124, no. 1, pp. 18–19, 2001.

[13] S. Griffith, "Growing machines," Ph.D. dissertation, MIT, 2004.

[14] K. C. Cheung, E. D. Demaine, J. R. Bachrach, and S. Griffith, "Programmable assembly with universally foldable strings (moteins)," *IEEE Transactions on Robotics*, vol. 27, pp. 718–729, 2011.

[15] R. V. Martinez, C. R. Fish, X. Chen, and G. M. Whitesides, "Elastomeric origami: Programmable paper-elastomer composites as pneumatic actuators," *Advanced Functional Materials*, vol. 22, pp. 1376–1384, 2012.

[16] J. A. Rogers, T. Someya, and Y. Huang, "Materials and mechanics for stretchable electronics," *Science*, vol. 327, pp. 1603–1607, 2010.

[17] R.-H. Kim, D.-H. Kim, J. Xiao, B. H. Kim, S.-I. Park, B. Panilaitis, R. Ghaffari, J. Yao, M. Li, Z. Liu, V. Malyarchuk, D. G. Kim, A.-P. Le, R. G. Nuzzo, D. L. Kaplan, F. G. Omenetto, Y. Huang, Z. Kang, and J. A. Rogers, "Waterproof AlInGaP optoelectronics on stretchable substrates with applications in biomedicine and robotics," *Nature materials*, vol. 9, pp. 929–937, 2010.

[18] M. Kaltenbrunner, T. Sekitani, J. Reeder, T. Yokota, K. Kuribara, T. Tokuhara, M. Drack, R. Schwodiauer, I. Graz, S. Bauer-Gogonea, S. Bauer, and T. Someya, "An ultra-lightweight design for imperceptible plastic electronics," *Nature*, vol. 499, pp. 458–463, 2013.

[19] D.-H. Kim, J.-H. Ahn, W. M. Choi, H.-S. Kim, T.-H. Kim, J. Song, Y. Y. Huang, Z. Liu, C. Lu, and J. A. Rogers, "Stretchable and foldable silicon integrated circuits," *Science*, vol. 320, pp. 507–511, 2008.

[20] P. Roberts, D. D. Damian, W. Shan, T. Lu, and C. Majidi, "Soft-matter capacitive sensor for measuring shear and pressure deformation," in *IEEE International Conference on Robotics and Automation (ICRA)*, 2013.

[21] J. K. Paik, R. K. Kramer, and R. J. Wood, "Stretchable circuits and sensors for robotic origami," in *IEEE/RSJ International Conference on Intelligent Robots and Systems*, 2011.

[22] L. V. der Pauw, "A method of measuring specific resistivity and hall effect of discs of arbitrary shape," Philips Research Reports, Tech. Rep. 13, 1958.

[23] H. A. Wheeler, "Inductance formulas for circular and square coils," *Proceedings of the IEEE*, vol. 70, no. 12, pp. 1449–1450, 1982.

[24] D. R. Frutiger, K. Vollmers, B. E. Kratochvil, and B. J. Nelson, "Small, fast, and under control: wireless resonant magnetic micro-agents," *International Journal of Robotics Research*, vol. 13, pp. 1–24, 2009.